

Flexible Polymer Sensors for *In Vivo* Intravascular Shear Stress Analysis

Hongyu Yu, Lisong Ai, Mahsa Rouhanizadeh, Darhsin Patel, Eun Sok Kim, and Tzung K. Hsiai

Abstract—Hemodynamic forces, specifically fluid shear stress, play an important role in the focal nature of arterial plaque formation known as atherosclerosis. We hereby developed biocompatible and flexible intravascular microelectromechanical systems sensor to measure real-time shear stress in the aortas of New Zealand White (NZW) rabbits. Titanium (Ti) and platinum (Pt) were deposited on silicon wafers and patterned to form the sensing elements. The polymer, parylene C, provided insulation to the electrode leads and flexibility to the sensors. Based on heat transfer principle, the heat dissipation from the sensors to the blood flow altered the resistance of the sensing elements, from which shear stress was calibrated. The resistance of the sensing element was measured at approximately 1.0 k Ω , and the temperature coefficient of resistance was at approximately 0.16%/°C. The individual sensors were packaged to the catheter for intravascular deployment in the aortas of NZW rabbits ($n = 5$). The sensor was capable of resolving spatial- and time-varying components of shear stress in the abdominal aorta. Computational fluid dynamic code based on non-Newtonian fluid properties showed comparable results within an acceptable range of experimental errors ($\pm 9\%$) for the maximal and minimal values in shear stress during one cardiac cycle. Therefore, we demonstrated the capability of biocompatible sensors for real-time shear stress measurement *in vivo* with a potential to advance the understanding between the blood flow and vascular disease. [2007-0291]

Index Terms—Microelectromechanical systems (MEMS) sensors, polymer, rabbit arterial circulation, shear stress.

I. INTRODUCTION

CORONARY heart disease remains the leading cause of death worldwide according to the World Health Organization [1]. Hemodynamic forces, specifically fluid shear stress, play an important role in the development of coronary artery disease [2]–[7]. The development of microelectromechanical systems (MEMS) sensors provides an entry point for assess-

ment of small-scaled hemodynamics with high spatial and temporal variations [8] otherwise difficult with computed tomography, magnetic resonance imaging, ultrasound, and laser Doppler velocimetry.

Fluid shear stress (τ) is a frictional force per unit area that is tangential to the surface of vascular endothelial cells. For a Newtonian fluid at steady state, shear stress is defined as

$$\tau = \mu \frac{du}{dy} \quad (1)$$

where μ represents viscosity and du/dy is the vertical velocity gradient along the y -axis perpendicular to the wall surface [9]. Two main methods for shear stress measurement have been developed. The first is to build a floating sensing element [10]. The advantage of such a design is direct measurements rather than indirect correlations between shear stress and other parameters, such as heat transfer. However, the sensing elements of floating sensors are fragile and usually difficult to fabricate. Their operation requires additional mechanical devices to amplify signal transduction in response to minute movements. The second is thermal anemometry [11]. The operation principle is based on convective cooling of a heated sensing element as fluid flows over its surface (Fig. 1). The heat transfer from the heated surface to the fluid depends on the flow characteristics in the viscous region of the boundary layer [12]. The advantages of this technique are simplicity in fabrication, absence of moving elements, and good sensitivity. Thus, the latter method provides a basis to develop micro intravascular sensors on a single silicon wafer for high-throughput production.

MEMS shear stress sensors have been developed for aerodynamics and fluid mechanics [11], [12]. A flexible shear-stress-sensor skin containing a 1-D array of 36 shear stress sensors has been designed to acquire shear stress measurement on the nonplanar surfaces [13]. We have previously fabricated MEMS shear stress sensor with backside wire bonding to address microscale hemodynamics with high temporal and spatial resolutions [8]. However, to assess shear stress in the complicated arterial geometry in the presence of time-varying component of blood flow, we hereby developed a new generation of polymer-based sensors that are flexible, biocompatible, and deployable into the arterial system.

Titanium (Ti) and platinum (Pt) layers embedded in the flexible polymer were used as the sensing elements. Based on heat transfer principle, heat convection from the resistively heated element to the flowing fluid is measured as a function of the changes in voltage, from which shear stress can be inferred [12]. The sensor was fabricated by surface micromachining

Manuscript received December 6, 2007; revised March 28, 2008. First published September 3, 2008; current version published October 1, 2008. The work of H. Yu was supported by American Heart Association (AHA) Postdoctoral Fellowship 0725016Y. The work of T. K. Hsiai was supported by American Heart Association GIA 0655051Y, NIH HL 83015, and NIH HL068689. The work of M. Rouhanizadeh was supported by AHA Predoctoral Fellowship 0615063Y. Subject Editor C. Liu.

H. Yu is with the School of Earth and Space Exploration and the Department of Electrical Engineering, Arizona State University, Tempe, AZ 85287 USA (e-mail: hongyuyu@asu.edu; hongyuyu@gmail.com).

L. Ai, M. Rouhanizadeh, and T. K. Hsiai are with the Department of Biomedical Engineering and the Division of Cardiovascular Medicine, University of Southern California, Los Angeles, CA 90089 USA.

D. Patel is with the Department of Biomedical Engineering, Georgia Institute of Technology, Atlanta, GA 30332-0250 USA.

E. S. Kim is with the Department of Electrical Engineering, University of Southern California, Los Angeles, CA 90089 USA.

Color versions of one or more of the figures in this paper are available online at <http://ieeexplore.ieee.org>.

Digital Object Identifier 10.1109/JMEMS.2008.927749

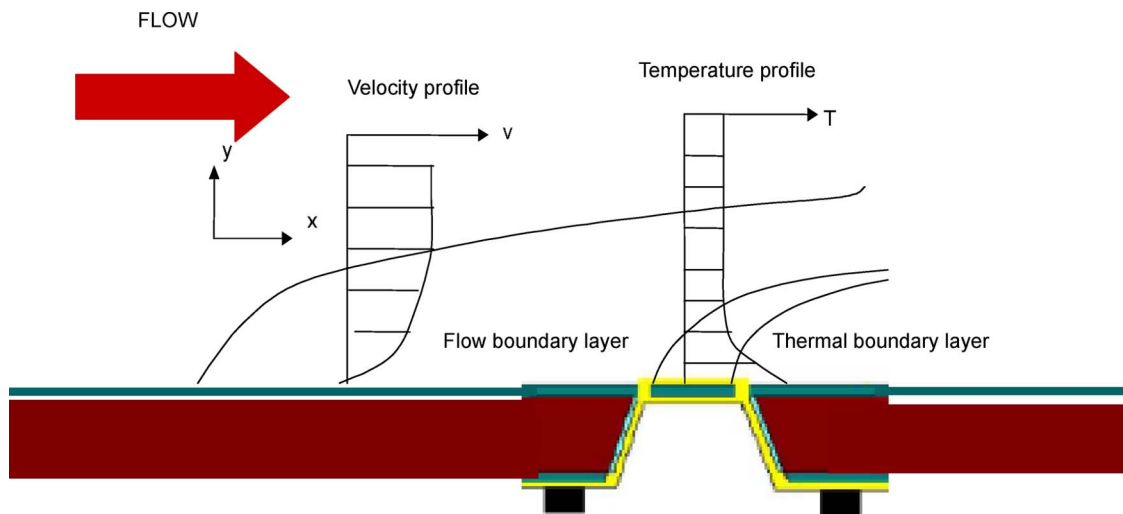


Fig. 1. Principle of thermal shear stress sensor. The thermal element resides within a flow velocity boundary layer. The rate of heat loss from a heated resistive element to the fluid flow is dependent on the velocity profile in the flow boundary layer. A thermal boundary develops beneath the flow velocity boundary layer. In this situation, convective heat transfer is related to changes in resistivity of the sensor, from which wall shear stress is calibrated [28].

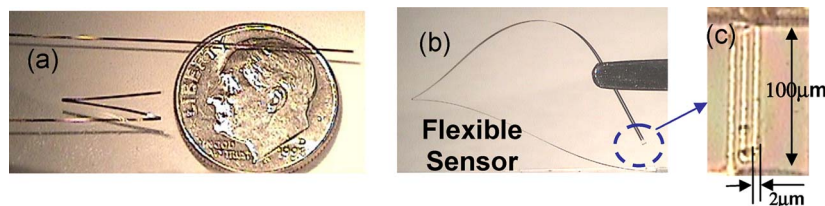


Fig. 2. Flexible intravascular sensors. (a) The sensor was bent or folded in a zigzag fashion without structural or functional damage. (b) The sensor was measured at 4 cm in length, $320\ \mu\text{m}$ in width, and $21\ \mu\text{m}$ in thickness. (c) The sensing element was positioned at the tip of the sensor, and the sensing element was made of $2\text{-}\mu\text{m}$ -wide Ti/Pt strip with a dimension of $280\ \mu\text{m}$.

technique utilizing parylene C as electrical insulation layer. The polymer-embedded sensor enables conformability to the geometry of arterial bifurcations and curvatures while retaining its mechanical strength and operational function. The resistance of the sensing element was measured at approximately $1.0\ \text{k}\Omega$, and the temperature coefficient of resistance (TCR) was at approximately $0.16\%/^{\circ}\text{C}$. The sensing element was connected to a flexible electrical coaxial wire that transmitted the changes in resistance to the external circuitry (Fig. 2). The position of the sensors in the aorta of the animal model was visualized under fluoroscope.

Direct measurement of wall shear stress in the aorta allows for prediction of the presence of plaque formation. We proposed to translate the MEMS-based technology from *in vitro* investigation of vascular biology to that of *in vivo* approach. Our sensor design addressed the following: 1) hemocompatibility and hemostasis of the sensor function in the rabbit blood and 2) integration of sensors with the catheter to transmit voltage signals to the external electronics. We demonstrate that the flexible and biocompatible polymer-based sensor allowed for direct real-time shear stress analysis in the abdominal aortas of NZW rabbits. The direct shear stress measurement agreed with that of the computational hemodynamics (CFD) code within an acceptable range of experimental differences. Thus, the polymer-based sensors provided a basis to investigate the interplay between hemodynamics and arterial plaque formation with a potential for clinical diagnostics.

II. METHODS

A. Microfabrication

The sensor was fabricated using surface micromachining with biocompatible materials including parylene C, Ti, and Pt. To dovetail to the arterial circulation, we have fabricated the sensors with the following: 1) dry thermal growth of $0.3\text{-}\mu\text{m}$ SiO_2 and deposition of a $1\text{-}\mu\text{m}$ sacrificial silicon layer using electron-beam (e-beam) evaporator; 2) deposition and patterning of Ti/Pt layers with thickness of $0.06\ \mu\text{m}/0.015\ \mu\text{m}$ for the sensing element with e-beam evaporator; 3) deposition of $9\text{-}\mu\text{m}$ parylene C with parylene vacuum coating system (PDS2010, Specialty Coating Systems, Inc., IN); 4) deposition and patterning of a metal layer of Cr/Au for electrode leads ($2\ \mu\text{m}$) with e-beam evaporator; 5) deposition and patterning of another thick layer of parylene C ($12\ \mu\text{m}$) to form the device structure; and 6) etching the underneath silicon sacrificial layer with XeF_2 dry etching system leading to the final device (Fig. 3). The resulting sensor bodies were 4 cm in length, $320\ \mu\text{m}$ in width, and $21\ \mu\text{m}$ in thickness (Fig. 2). The fabrication process illustrates the application of Ti and Pt as the heating and sensing elements [Fig. 3(f)]. The Ti/Pt sensing elements (strip of $280\ \mu\text{m}$ in length by $2\ \mu\text{m}$ in width) were encapsulated with parylene which was in direct contact with the blood flow. They offer low resistance drift, large range of thermal stability, low $1/f$ noise in the absence of piezoresistive effect, and resistance to corrosion/oxidation [14], [15].

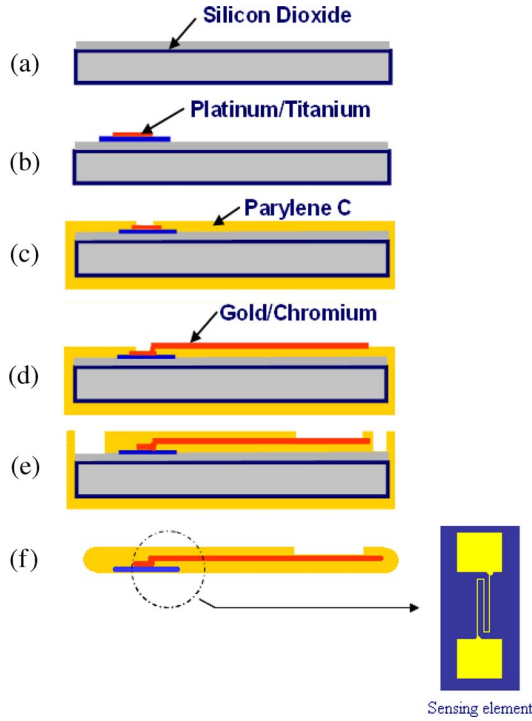


Fig. 3. Fabrication process of the sensor. (a) Thermal growth of SiO_2 and deposition of sacrificial Si layer ($1 \mu\text{m}$). (b) Deposition and patterning of Ti/Pt layers ($0.06 \mu\text{m}/0.015 \mu\text{m}$) for the sensing element. (c) Deposition of parylene C ($9 \mu\text{m}$). (d) deposition and patterning of a metal layer of Cr/Au for electrode leads ($2 \mu\text{m}$). (e) Deposition and patterning of a thick layer of parylene C ($12 \mu\text{m}$) to form the device structure. (f) Etching the underneath Si sacrificial layer leading to the final device.

B. Catheter-Based Polymer Sensors

The sensors were integrated to an electrical coaxial wire as catheter's guide wire application for intravascular shear stress analysis (Fig. 4). The Cr/Au electrode leads were connected to an electrical coaxial wire (Precision Interconnect, Portland, OR) by using the biocompatible conductive epoxy (H20E, www.epotek.com) that was cured at 90°C over 3 h. The electrical coaxial wire allowed for the electrical-signal transmission from the arterial circulation to the external circuitry. The sensor was mounted to the coaxial wire at 4 cm from the tip analogous to the entrance length required to deliver well-defined laminar flow field. This distance avoided flow disturbance at the tip of the coaxial wire. The biocompatible epoxy anchored the sensing elements on the coaxial-wire surface. The coaxial wire was 0.4 mm in diameter, and the sensing element was $80 \mu\text{m}$ in width and $240 \mu\text{m}$ in length. Using the fluoroscope in the animal angiographic laboratory, the operator was able to visualize and steer the sensor wire in the aorta of New Zealand White (NZW) rabbits to the anatomic regions of interest, namely, aortic arch and abdominal aorta [Fig. 5(a)]. Contrast dye was injected to delineate the position of the wire in relation to the inner diameter of the aorta [Fig. 5(b)]. Simultaneously, the catheter-based sensor was rotated to ensure that the sensing element was facing the blood flow rather than the wall, based on the distinct difference in the voltage signals detected with the sensing element facing the wall and the blood flow (Fig. 6).

C. Calibration of the Polymer Sensors

Based on the heat transfer principle, the output voltage of the MEMS sensors under the constant current detection circuits was sensitive to the fluctuation in ambient temperature (Fig. 1). The temperature overhear ratio (α_T) is defined as temperature variations of the sensor over the ambient temperature (T_0) [11]

$$\alpha_T = \frac{(T - T_0)}{T_0} \quad (2)$$

where T denotes the temperature of the sensor. The relation between resistance and temperature overhear ratios is expressed as

$$\alpha_R = \frac{(R - R_0)}{R} = \alpha(T - T_0) \quad (3)$$

where α is the TCR. For shear stress measurement, we applied a high overhear ratio ($\sim 3\%$) by passing higher current and by generating a "hot" sensing element to stabilize the sensor. Calibration was performed in a 2-D flow channel for individual sensors to establish a relationship between heat exchange (from the heated sensing element to the flow field) and shear stress over a range of steady flow rates (Q_n) in the presence of rabbit blood flow at 37.8°C (Fig. 7).

For a Newtonian fluid at steady state, the theoretical shear stress value in relation to the flow rate in the 2-D flow channel was established using the following formula based on the analysis of Truskey *et al.* [29]:

$$\begin{aligned} \tau_{xy} \Big|_{y=\frac{H}{2}, x=0} \\ = \mu Q \cdot \frac{6 - \sum_{n=0}^{\infty} \frac{48}{(2n+1)^2 \pi^2 \cosh\left(\frac{(2n+1)\pi W}{2H}\right)}}{WH^2 - \sum_{n=0}^{\infty} \frac{96H^3}{(2n+1)^5 \pi^5 \cosh\left(\frac{(2n+1)\pi W}{2H}\right)} \cdot \exp\left(\frac{(2n+1)\pi W}{2H}\right)} \\ y \in \left(-\frac{H}{2}, \frac{H}{2}\right), \quad x \in \left(-\frac{W}{2}, \frac{W}{2}\right) \end{aligned} \quad (4)$$

where τ_w is the wall shear stress, μ is the blood viscosity, and H and W are the height and the width of the flow channel, respectively ($H/W = 0.433$). The viscosity used in the aforementioned equation was obtained from the published data for rabbit blood [16]. The individually calibrated sensors were then deployed to the NZW rabbit's aorta for real-time shear stress assessment.

D. In Vivo Assessment of Intravascular Shear Stress

We tested the feasibility of acquiring real-time shear stress measurements from the NZW rabbit's aorta, specifically abdominal aorta and aortic arch (Fig. 8). Deployment of the polymer device into the rabbit's aorta was performed in compliance with the Institutional Animal Care and USC Committee in the Heart Institute of Good Samaritan Hospital, Los Angeles, which is accredited by the American Association for Accreditation for Laboratory Animal Care.

Five male NZW rabbits (10–12 weeks, with mean body weight of $2105 \pm 47 \text{ g}$) were acquired from a local breeder (Irish Farms, Norco, CA) and maintained by the USC vivaria in

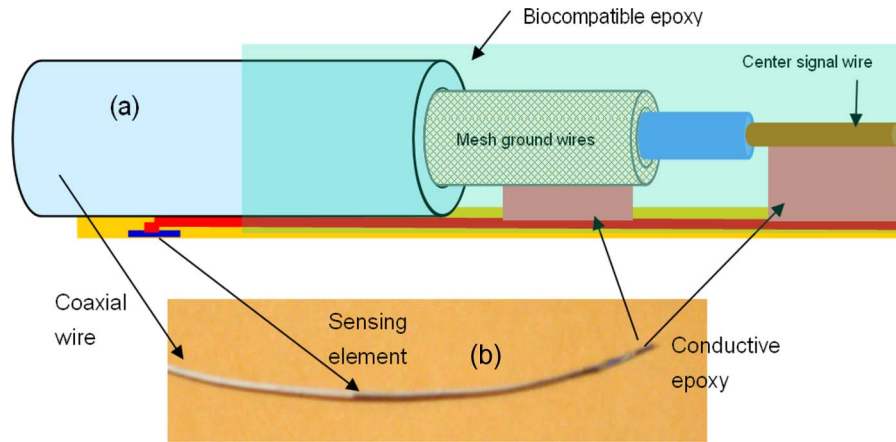


Fig. 4. Packaging of the polymer shear stress sensor. (a) The sensor was connected to the electrical coaxial wire with conductive epoxy and covered with biocompatible epoxy to prevent electrical current leakage. The distance between the sensing element and the tip of the catheter was 4 cm which was based on entrance length to avoid flow disturbance [24]. (b) (Black color) Packaged sensor on (white color) electrical coaxial wire.

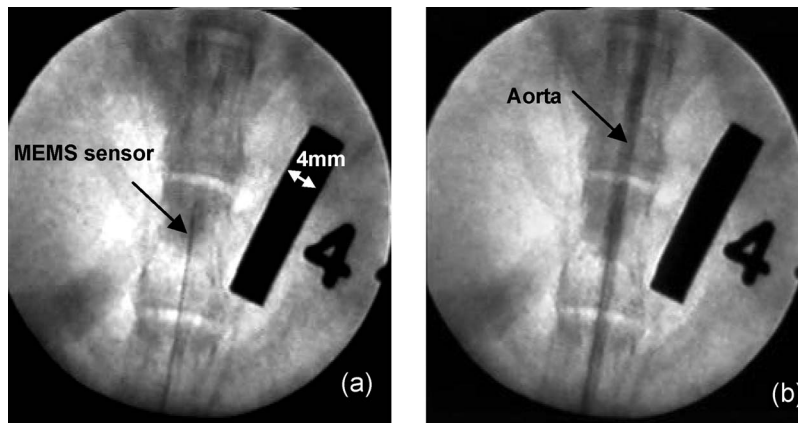


Fig. 5. Fluoroscope images of *in vivo* testing of the MEMS sensor. (a) Catheter-based MEMS polymer sensor in the abdominal aorta of the NZW rabbit in the absence of contrast dye. (b) The contrast dye was injected to delineate the diameter of the aorta in relation to that of the catheter.

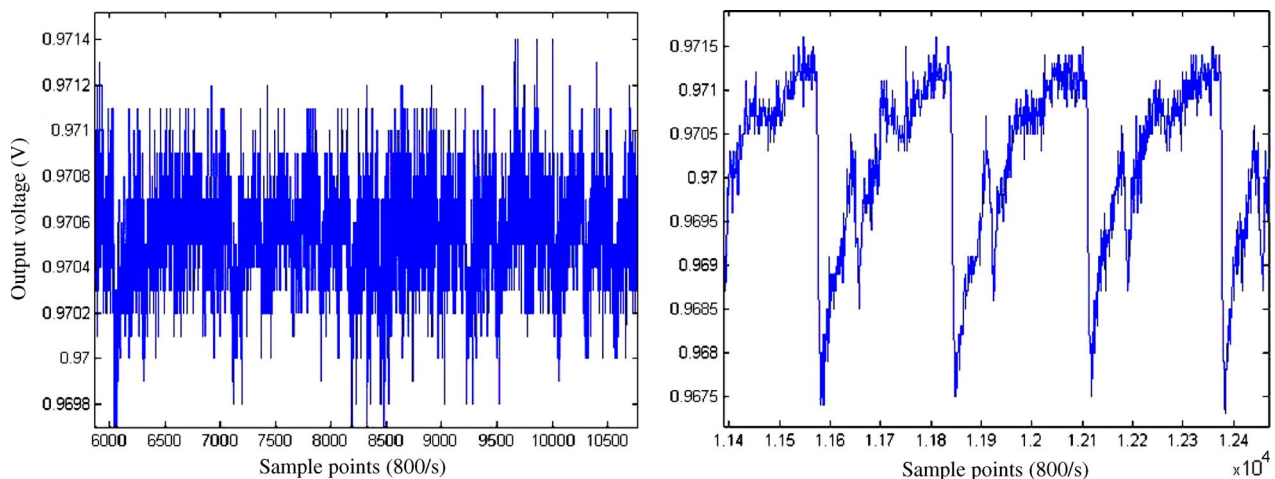


Fig. 6. Sensor's output voltage signals. (a) The sensing element was facing the arterial wall. (b) The sensing element was facing the flow field.

accordance with the National Institutes of Health guidelines. After a seven-day quarantine period, the rabbits were anesthetized for percutaneous access according to the institutional review committee, and anesthesia was induced with an intramuscular injection of 100-mg/kg ketamine (Fort Dodge Laboratories, Inc.) combined with 1-mg/kg acepromazine (Aveco

Company). A 23-gauge hypodermic needle and a 26-gauge guide wire were introduced into the left femoral artery via a cut-down. A rabbit femoral catheter (0.023" ID × 0.038" OD) was passed through the left femoral artery, where electrical coaxial wire packaged with sensor passed through. The circulatory system of the individual animals was heparinized (100 U/kg

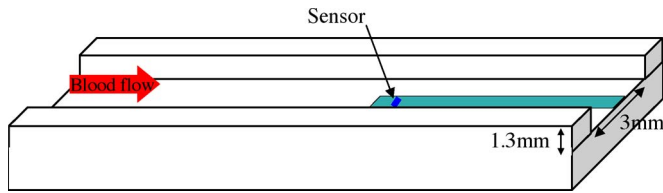


Fig. 7. Schematic diagram of 2-D micro PDMS channel for sensor calibration in the rabbit blood. The sensor body was flush-mounted on the floor of the channel at a sufficient entrance length to allow for fully developed laminar flow before reaching the sensor.

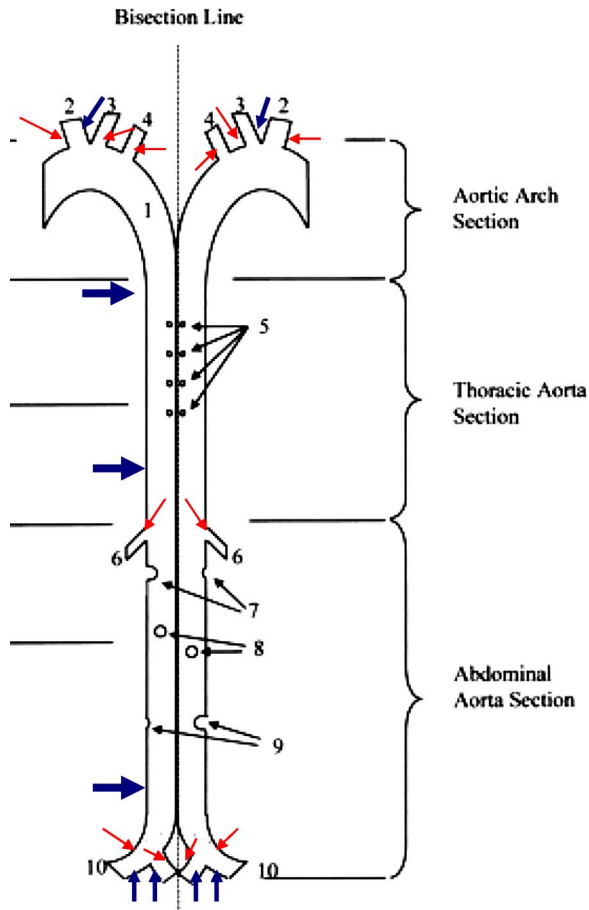


Fig. 8. Diagram (not drawn to scale) showing the bisection of the aorta and the division of aortic segments from the NZW rabbit. 1—The aorta. 2—Brachiocephalic trunk. 3—Common carotid artery (which sometimes branches from the brachiocephalic trunk). 4—Left subclavian artery. 5—Dorsal intercostal arteries. 6—Celiac artery. 7—Cranial mesenteric artery. 8—Right and left renal arteries. 9—Caudal mesenteric artery. 10—Iliac arteries. The red arrows indicate the loci where disturbed flow, including oscillatory flow, occurs. The blue arrows indicate the regions where pulsatile flow develops. Our flexible sensors were positioned in the abdominal aorta section below the celiac arteries.

prior to sensor deployment. The catheters and needles were rinsed with heparin at 1000 U/mL prior to the procedure.

Under the fluoroscopic guidance (Phillips BV-22HQ C-arm), the catheter integrated with the micro vascular device was deployed into the abdominal aorta above the renal arteries for shear stress measurements under fluoroscopy guidance (Fig. 5). Periodic blood pressure measurement was obtained with an automated tail cuff (IITC/Life Science Instruments). The shear stress recordings were synchronized with the rabbit's cardiac cycle via ECG (The ECGenie, Mouse Specifics). After mea-

surement, the catheter was removed, and the femoral artery was tied off.

The position of the catheter in relation to the arterial wall was visualized via the contrast dye under fluoroscope. The output voltage of the sensor was high when the sensor was facing the blood, whereas the signal was attenuated as we steered the sensor toward the arterial wall. Unlike our previously published wall shear stress measurement for an *in vitro* bifurcating model [17], the unique feature of our catheter-based approach allowed for intravascular shear stress analysis in response to pulsatile blood flow in the abdominal aorta of the NZW rabbit.

E. Data Acquisition

The constant current circuit has been used to measure the shear stress in aorta. Electrical current of 0.9833 mA was input from a multimeter (HP34401A, Santa Clara, CA), which was working at resistance measurement mode. When the current passed through the sensor, the sensing element was heated up at an overheat ratio of $\sim 3\%$ and had a temperature increase by $\sim 9^\circ\text{C}$ at its focal point. This localized heating will not harm the blood biological activities. The reasons are as follows: The sensing element, which is the hottest spot (9°C above biological temperature), is very small at a few hundred micrometers in the flow direction, and the blood cells only need tens of milliseconds to pass the sensing element. Also, in arterial blood flow, blood cells aggregate toward the maximal velocity in the center and will be isolated from the hottest spot. The voltage across the sensing element was monitored by LabView data acquisition board (NI USB-6251, Austin, TX) and BNC adaptor board (BNC-2110, Austin, TX) which was connected to a laptop computer (Thinkpad T61, Lenovo, China). The main source of noise was electrical magnetic interference from the environment at 60 Hz. We analyzed the data to filter out 60-Hz noise and improved the noise floor from 1.2 to 0.5 mV. The sample rate for data acquisition was at 800 points/sec. The signal-to-noise ratio was 4.8.

F. Development of CFD Stimulation

1) *Generation of 3-D Geometries and Meshes:* Computational fluid dynamic (CFD) code was developed for non-Newtonian fluid to simulate real-time shear stress in the abdominal aorta and to compare with the experimental measurements. The luminal geometrical model of the rabbit abdominal aorta was constructed and meshed using a specialized preprocessing program GAMBIT (Fluent Inc., Gambit 2.3.16, Lebanon, NH) [18]. The local effects of branching arteries were assumed to be negligible. The meshed models were then imported into the main CFD solver FLUENT (Fluent Inc., Fluent 6.2.16, Lebanon, NH) [19] for pulsatile-flow simulation. The grid was generated by meshing the inlet surface using Pave scheme type to create unstructured mesh, followed by generating a volume mesh using Cooper scheme type to sweep the mesh node patterns that specified the inlet surface as the "source" faces. The model was composed of 174510 cells which were primarily the wedge elements. For simulation of wall shear stress, boundary layers immediately

adjacent to the wall were constructed to generate sufficient information for characterization of the large fluid velocity gradients near the wall. The diameter of the rabbit abdominal aorta, D , which was measured from angiography during sensor deployment, was set at 2.4 mm. The total length was set at 8.27 times of the diameter to provide sufficient entrance length for the flow to develop [20].

The pulsatile centerline flow velocity information was applied to compute a complex Fourier series approximation for the inlet flow rate pulse using Womersley solution [21]. The blood flow was simulated by applying the 3-D Navier–Stokes equations. The governing equations, including mass and momentum equations, were solved by the FLUENT software for laminar, incompressible, and non-Newtonian flow. The arterial wall of the rabbit abdominal aorta was assumed to be rigid and impermeable.

At the inlet of the abdominal aorta, a physiological flow waveform was introduced [22], [23]. The transient flow rate information was used to compute a complex Fourier series approximation for the pressure gradient pulse using Womersley solution [23]. This profile was implemented by the user-defined C++ code. The flow outlet was far downstream where traction-free condition was prescribed. This approach allowed the velocity profile to become a solution to the 3-D Navier–Stokes equations, and the velocity profile was propagated downstream along the aorta. No-slip boundary condition was implemented along the inner walls.

The flow field was initialized by propagating the constant time-averaged inlet velocity profile downstream into the computational domain. The initial pressure was set to zero in the entire domain, as were the two cross-stream velocity components. An iterative scheme that marched toward a converged solution was employed by FLUENT. The second-order implicit formulation of the solver was applied for the unsteady simulations. Second-order upwind discretization was applied for the governing equations. The pressure–velocity coupling was based on the SIMPLEC technique.

III. RESULTS

A. Properties of Polymer Sensors

The resistance of the sensing element was approximately $1.0\text{ k}\Omega$, and the TCR was measured to be approximately $0.16\%/^{\circ}\text{C}$ (Fig. 9). These properties were compatible for *in vivo* analysis. The relation between the resistance and temperature was linear, suggesting that the TCR over this temperature range remained constant.

B. Calibration of the Polymer Sensors

To account for the non-Newtonian properties of the blood flow, we collected 10-mL blood from the NZW rabbits, added EDTA as anticoagulant, and then assessed the dynamic range of viscosity at $37.8\text{ }^{\circ}\text{C}$ in a 2-D flow channel (Fig. 7). The blood viscosity decreased exponentially as the shear rates increased. At shear rate greater than 1000, the viscosity became asymptotic. The sensing element ($240 \times 80 \times 0.1\text{ }\mu\text{m}^3$) was

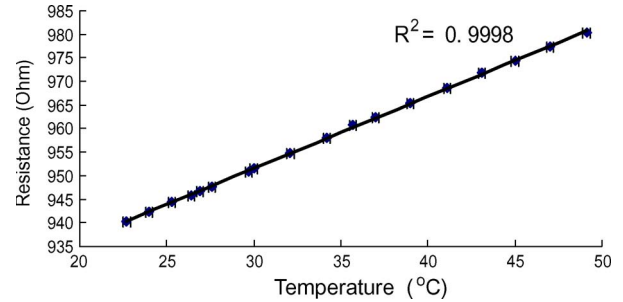


Fig. 9. Plot of sensing element (Ti/Pt) resistance versus temperature. A linear relation was established over the temperature ranging from $22\text{ }^{\circ}\text{C}$ to $50\text{ }^{\circ}\text{C}$. The TCR was approximately $0.16\%/^{\circ}\text{C}$.

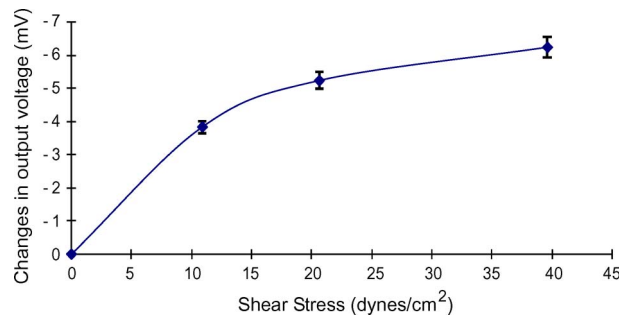


Fig. 10. Calibration curve for changes in sensor output voltage and shear stress in response to the rabbit blood flow. Output voltage was plotted as a function of wall shear stress in the PDMS channel. A constant current mode was driving the sensor. As shear stress increased, the rate of heat dissipation to the flow field increased, resulting in a decrease in resistivity of the sensor. Given the relation of V (voltage) = I (current) \times R (resistance), the output voltage decreased.

positioned in a polydimethylsiloxane (PDMS) flow channel (1.32 mm high and 3.0 mm wide) for sensor calibration in the presence of rabbit blood flow at $37.8\text{ }^{\circ}\text{C}$. We obtained a nonlinear relation between changes in sensor output voltage as a result of heat dissipation from the sensing element to the blood flow field as a function of shear stress (Fig. 10). When the sensor reached the thermal equilibrium status, the following relation developed:

$$P_e = P_b(\Delta T) + P_f(\Delta T, \tau)$$

where P_e is the input electrical power, P_b is the power contained in the sensor body, and ΔT is the change in temperature of the sensor in response to fluid flow. ΔT was derived from the output voltage of the constant current-mode circuit, and τ is the shear stress. This equation shows the direct relation between the output voltage and shear stress τ , as shown in Fig. 10. Thus, this calibration curve allowed for conversion of voltage signals acquired from the abdominal aorta to shear stress.

IV. *IN VIVO* ASSESSMENT OF INTRAVASCULAR SHEAR STRESS

A. Conversion of Voltage Signals to Shear Stress in the Abdominal Aorta

The intravascular shear stress in the abdominal aorta was obtained using the calibration curve, as shown in Fig. 10.

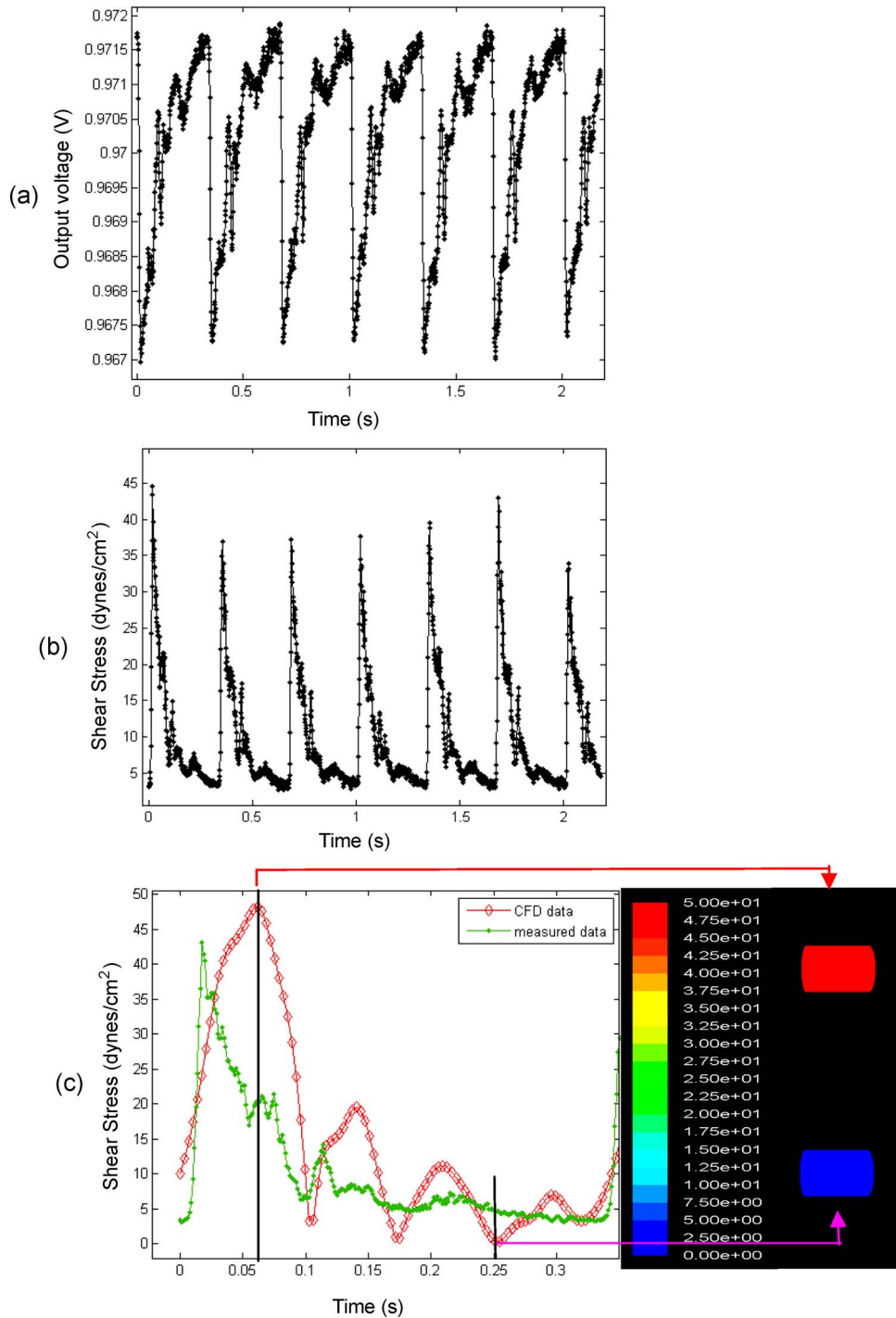


Fig. 11. Conversion of output voltage to shear stress. (a) Real-time voltage signals were obtained from the abdominal aorta of NZW rabbits. (b) Shear stress profile was converted from the measured output voltage profile. (c) (In green) Shear stress tracing in one cardiac cycle was compared with CFD simulation. The color scale revealed the instantaneous wall shear stress at the maximal and minimal points.

The real-time output voltage was recorded at 800 sample points/sec and a noise floor of 0.5 mV in response to pulsatile flow at approximately 180 beats/min. Shown in Fig. 11(a) is a representative output voltage tracing over six cardiac cycles with an interval of 0.33 s/heart beat in the abdominal aorta. Shown in Fig. 11(b) is the corresponding intravascular shear stress profile over six cardiac cycles. Superimposed with the experimental shear stress value (green) is the CFD solution (red) [Fig. 11(c)]. The measured shear

stress peaked at 44 dyn/cm² during systole and bottomed at 5 dyn/cm² during diastole. The noise floor was approximately 1 dyn/cm² [Fig. 11(c)]. The CFD solution revealed a peak wall shear stress value at 48 dyn/cm². Despite the distinct waveforms between the intravascular shear stress (experimental) and wall shear stress (CFD simulation), the two peak values varied by 9%, and the waveform profiles overlapped within the range of acceptable experimental errors for wall shear stress measurement [4].

V. DISCUSSION

In this paper, we demonstrate the first flexible polymer sensors to acquire real-time shear stress measurement *in vivo* with a potential for clinical applications. The feasibility to translate micro device for *in vivo* real-time analysis represents an advance in the field of MEMS technology to contribute to the understanding of hemodynamics and vascular disease. Our sensor design successfully addressed the following: 1) hemocompatibility and hemostasis of the sensor function in the rabbit blood and 2) integration of sensors with the catheter to transmit voltage signals to the external electronics. Distinct from our previous MEMS shear stress sensor prototypes were the application of titanium and platinum for the sensing element and the use of parylene C to provide both insulation of electrodes and flexibility of the sensors. Unlike our previously published wall shear stress measurement for an *in vitro* bifurcating model [8], the unique feature of our catheter-based approach allowed for intravascular shear stress analysis in response to pulsatile blood flow in the abdominal aorta of the NZW rabbit. Despite the varied waveforms, the intravascular shear stress analysis in the abdominal aorta overlapped with that of the wall shear stress by CFD code with experimental error at 9%. Due to the fact that the blood viscosity near the vessel wall is not precisely known, the wall shear stress measurement can be off by 20%–50% [4]. Thus, the 9% error is within the range of acceptable shear stress measurement.

Several reasons accounted for the distinct waveforms between the experimental and CFD solutions. The experimental data were acquired from anesthetized rabbits with an average heart rate of 180 beats/min. The anatomy of the rabbit abdominal aorta contained multiple branches (7, 8, and 9 in Fig. 8). The focal effects of small branches were assumed to be negligible for the CFD code. Another uncertainty in calibrating the sensors in the presence of non-Newtonian fluid is viscosity. In considering the rheological properties of blood, the viscosity obtained for the rabbit blood varied under the conditions of measurement such as the use of viscometer, presence of EDTA to prevent coagulation of blood, temperature, and hematocrit ratio (ratio of volume of red blood cells to volume of the whole blood) [24]. For a given hematocrit ratio, the apparent viscosity of blood is less when measured in a viscometer than in conventional capillary tube viscometer [25]. Despite the use of published data for viscosity [16], the viscosity of blood was dependent on the diameter of aorta and shear rate in our measurement. The greater tendency of the red blood cells to accumulate in the axial laminae at higher flow rate is partly responsible for the phenomenon known as shear thinning. The third reason is the catheter-based sensor allowed for “intravascular” shear stress analysis, whereas the CFD codes simulated the “wall” shear stress measurement. Thus, both the anatomy of aorta and the apparent viscosity in the abdominal aorta influence the relative difference between our experimental measurement and the CFD codes.

The signal-to-noise ratio is important for *in vivo* application. The sensitivity of the MEMS sensors was experimentally measured by $\Delta v/v$ or $\Delta v/\Delta\tau$ from experimental data (calibration curves). v and τ denote the voltage and the shear stress, respec-

tively. The reported sensitivity by Chandrasekaran *et al.* [26] was in the range of 11 mV/Pa or 1.1 mV/(dyn/cm²). The use of Ti and Pt as sensing element materials provides biocompatibility but accounts for a maximum sensitivity of 0.35 mV/(dynes/cm²).

Both polysilicon and platinum have been used as the sensing elements of the MEMS sensors. Polysilicon is an ideal semiconductor because of the following reasons: 1) uniform deposition property; 2) a relatively high TCR; and 3) a high resistance (when undoped) as a sensing element. Therefore, the sensitivity of polysilicon-based shear stress sensor is high. In contrast, titanium (Ti) and platinum (Pt) have lower impedance or relatively lower sensitivity. However, Ti and Pt harbor low $1/f$ noise (f = frequency), in the absence of piezoresistively induced pressure signal, in the polysilicon-based resistor. Furthermore, Ti and Pt are resistant to corrosion and oxidation. They are thermally stable over a wide range of temperature. The low deposition temperature is compatible with parylene technology. Unlike the polysilicon that is uniformly deposited by low-pressure chemical vapor deposition at 600 °C, platinum is typically deposited by either e-beam evaporation or electroplating at room temperature (Fig. 1). Therefore, the microfabrication for our polymer-based sensors is less complicated compared with that for the previous MEMS shear stress sensors [27].

In summary, this pilot study enabled us to assess the characteristics of shear stress; namely, spatial and temporal variations and further enabled us to evaluate potential pitfalls surrounding issues with microfouling, hemocompatibility, and device noise in the animal models. The feasibility of translating the MEMS device for real-time and dynamic analysis paves the way to conduct long-term follow-up of our animal model in response to hypercholesterolemic diet and therapeutic intervention. In our future investigation, the changes in intravascular shear stress signal and waveforms will be compared prior and after high fat diet in the abdominal aorta above renal arterial bifurcation in our NZW rabbit model. Also, the simultaneous application of abdominal ultrasound will be used to further delineate the cross section of the aorta for the position of the sensor. The long-term goal is to embrace both physical and biochemical analyses of vascular hemodynamics to predict the individuals at risk for abdominal aortic aneurysm, acute coronary syndromes, and strokes.

ACKNOWLEDGMENT

The authors would like to thank E. Meng and P.-Y. Li for fabricating the 2-D flow channel.

REFERENCES

- [1] *Deaths From Coronary Heart Disease*. [Online]. Available: http://www.who.int/cardiovascular_diseases/en/cvd_atlas_14_deathHD.pdf
- [2] R. M. Nerem, R. W. Alexander, D. C. Chappell, R. M. Medford, S. E. Varner, and W. R. Taylor, “The study of the influence of flow on vascular endothelial biology,” *Amer. J. Med. Sci.*, vol. 316, no. 3, pp. 169–175, Sep. 1998.
- [3] J. N. Topper, J. Cai, D. Falb, and M. A. Gimbrone, Jr., “Identification of vascular endothelial genes differentially responsive to fluid mechanical stimuli: Cyclooxygenase-2, manganese superoxide dismutase, and endothelial cell nitric oxide synthase are selectively up-regulated by steady laminar shear stress,” *Proc. Nat. Acad. Sci. U.S.A.*, vol. 93, no. 19, pp. 10417–10422, Sep. 1996.

- [4] D. D. Ku, "Blood flow in arteries," *Annu. Rev. Fluid Mech.*, vol. 29, pp. 399–434, Jan. 1997.
- [5] P. F. Davies, C. F. Dewey, Jr., S. R. Bussolari, E. J. Gordon, and M. A. Gimbrone, Jr., "Influence of hemodynamic forces on vascular endothelial function. In vitro studies of shear stress and pinocytosis in bovine aortic cells," *J. Clin. Invest.*, vol. 73, no. 4, pp. 1121–1129, Apr. 1984.
- [6] J. V. Soulis, G. D. Giannoglou, Y. S. Chatzizisis, T. M. Farmakis, G. A. Giannakoulas, G. E. Parcharidis, and G. E. Louridas, "Spatial and phasic oscillation of non-Newtonian wall shear stress in human left coronary artery bifurcation: An insight to atherogenesis," *Coron. Artery Dis.*, vol. 17, no. 4, pp. 351–358, May 2006.
- [7] T. Frauenfelder, E. Boutsianis, T. Schertler, L. Husmann, S. Leschka, D. Poulikakos, B. Marincek, and H. Alkadhi, "Flow and wall shear stress in end-to-side and side-to-side anastomosis of venous coronary artery bypass grafts," *BioMed. Eng. OnLine*, vol. 6, p. 35, Sep. 2007.
- [8] M. Rouhanizadeh, G. Soundararajan, R. Lo, D. Arcas, F. Browand, and T. Hsiai, "MEMS sensors to resolve spatial variations in shear stress in a 3-D blood vessel bifurcation model," *IEEE Sensors J.*, vol. 6, no. 1, pp. 78–88, Feb. 2006.
- [9] Y. C. Fung, *Biomechanics: Circulation*, 2nd ed. New York: Springer-Verlag, 1997.
- [10] M. A. Schmidt, R. T. Howe, S. D. Senturia, and J. H. Haritonidis, "Design and calibration of a microfabricated floating-element shear-stress sensor," *IEEE Trans. Electron Devices*, vol. 35, no. 6, pp. 750–757, Jun. 1988.
- [11] Q. Lin, F. K. Jiang, X. Q. Wang, Y. Xu, Z. G. Han, Y. C. Tai, J. Lew, and C. M. Ho, "Experiments and simulations of MEMS thermal sensors for wall shear-stress measurements in aerodynamic control applications," *J. Micromech. Microeng.*, vol. 14, no. 12, pp. 1640–1649, Dec. 2004.
- [12] C. Liu, Y. C. Tai, J. B. Huang, and C. M. Ho, "Surface micromachined thermal shear stress sensor," in *Proc. 1st ASME Symp. Appl. Micro-Fabr. Fluid Mech.*, Chicago, IL, Nov. 1994, pp. 9–15.
- [13] Y. Xu, Y.-C. Tai, A. Huang, and C.-M. Ho, "IC-integrated flexible shear-stress sensor skin," *J. Microelectromech. Syst.*, vol. 12, no. 5, pp. 740–747, Oct. 2003.
- [14] E. Meng and Y. C. Tai, "A parylene MEMS flow sensing array," in *Proc. 12th Int. Conf. Solid State Sens., Actuators Microsyst.*, 2003, pp. 686–689.
- [15] A. Cain, T. Nishida, and M. Sheplak, "Development of a wafer-bonded, silicon-nitride membrane thermal shear-stress sensor with platinum sensing element," in *Proc. Solid-State Sens. Actuator Workshop*, Hilton Head Island, SC, 2000.
- [16] P. W. Longest, C. Kleinstreuer, G. A. Truskey, and J. R. Buchanan, "Relation between near-wall residence times of monocytes and early lesion growth in the rabbit aorto-celiac junction," *Ann. Biomed. Eng.*, vol. 31, no. 1, pp. 53–64, Jan. 2003.
- [17] M. Rouhanizadeh, L. Lin, D. Ascara, and T. Hsiai, "Spatial variations in Shear stress at low Reynolds number flow," *Ann. Biomed. Eng.*, vol. 33, no. 10, pp. 1425–1440, 2005.
- [18] *Gambit 2.3 User's Guide*, Fluent Inc., Lebanon, IN, 2006.
- [19] *FLUENT 6.2 User's Guide*, Fluent Inc., Lebanon, IN, 2006.
- [20] T. Kim, T. Seo, and A. I. Barakat, "Numerical simulations of fluid mechanical interactions between two abdominal aortic branches," *Korea-Aust. Rheol. J.*, vol. 16, no. 2, pp. 75–83, 2004.
- [21] J. R. Womersley, "Method for the calculation of velocity, rate of flow and viscous drag in arteries when the pressure gradient is known," *J. Physiol.*, vol. 127, no. 3, pp. 553–563, Mar. 1955.
- [22] C. A. Taylor, T. J. T. Hughes, and C. K. Zarins, "Finite element modeling of three-dimensional pulsatile flow in the abdominal aorta: Relevance to atherosclerosis," *Ann. Biomed. Eng.*, vol. 26, no. 6, pp. 975–987, Nov. 1998.
- [23] X. He, D. N. Ku, and J. E. Moore, "Simple calculation of the velocity profiles for pulsatile flow in a blood vessel using Mathematica," *Ann. Biomed. Eng.*, vol. 34, no. 1, pp. 45–49, Jan. 1993.
- [24] R. M. Berne and M. N. Levy, *Cardiovascular Physiology*, 8th ed. St. Louis, MO: Mosby, pp. 127–132.
- [25] M. N. Levy and L. Share, "The influence of erythrocyte concentration upon the pressure–flow relationships in the dog's hind limb," *Circ. Res.*, vol. 1, no. 3, p. 247, May 1953.
- [26] V. Chandrasekaran, A. Cain, T. Nishida, L. Cattafesta, and M. Sheplak, "Characterization of a micromachined thermal shear stress sensor," presented at the 39th AIAA Aerospace Sciences Meeting, Reno, NV, Jan. 2001, AIAA Paper 2001-0247.
- [27] T. Hsiai, A. Salazar, M. A. Ing, S. K. Cho, P. K. Wang, M. Navab, L. Demer, and C. M. Ho, "Micro sensors: Linking real-time inflammatory responses with oscillatory shear stress," *Ann. Biomed. Eng.*, vol. 32, no. 2, pp. 189–201, Feb. 2004.
- [28] C. M. Ho and Y. C. Tai, "Micro-electro-mechanical systems and fluid flows," *Annu. Rev. Fluid Mech.*, vol. 30, pp. 579–612, Jan. 1998.
- [29] G. Truskey, F. Yuan, and D. Katz, *Transport Phenomena in Biological Systems*. Upper Saddle River, NJ: Pearson Prentice Hall, 2004.

Hongyu Yu, photograph and biography not available at the time of publication.

Lisong Ai, photograph and biography not available at the time of publication.

Mahsa Rouhanizadeh, photograph and biography not available at the time of publication.

Darhsin Patel, photograph and biography not available at the time of publication.

Eun Sok Kim, photograph and biography not available at the time of publication.

Tzung K. Hsiai, photograph and biography not available at the time of publication.